BIOCHEMISTRY
including biophysical chemistry & molecular biology

Article

pubs.acs.org/biochemistry

Light−Dark Adaptation of Channelrhodopsin Involves Photoconversion between the all-*trans* and 13-*cis* Retinal Isomers

Sara Bruun,[†] Daniel Stoeppler,[‡] Anke Keidel,[†] Uwe Kuhlmann,[†] Meike Luck,[§] Anne Diehl,[‡] Michel-Andreas Geiger,[‡] David Woodmansee,[∥] Dirk Trauner,[∥] Peter Hegemann,[§] Hartmut Oschkinat,*[,‡] Peter Hildebrandt,*[,†] and Katja Stehfest*[,§]

[†]Technische Universität Berlin, Institut für Chemie, Sekr. PC14, Straße des 17. Juni 135, D-10623 Berlin, Germany

[‡]Leibniz-Institut für Molekulare Pharmakologie (FMP), Robert-Rössle-Strasse 10, 13125 Berlin, Germany

[§]Humboldt-Universität zu Berlin, Institut für Biologie, Invalidenstrasse 42, D-10115 Berlin, Germany

[∥]Department of Chemistry, Ludwig-Maximilians-Universität München, Butenandtstraße 5-13, 81377 München, Germany

Supporting Information

ABSTRACT: Channelrhodopsins (ChR) are light-gated ion channels of green algae that are widely used to probe the function of neuronal cells with light. Most ChRs show a substantial reduction in photocurrents during illumination, a process named "light adaptation". The main objective of this spectroscopic study was to elucidate the molecular processes associated with light−dark adaptation. Here we show by liquid and solid-state nuclear magnetic resonance spectroscopy that the retinal chromophore of fully dark-adapted ChR is exclusively in an all-*trans* configuration. Resonance Raman (RR) spectroscopy, however, revealed that already low light intensities establish a photostationary equilibrium between all-*trans*,15-*anti* and 13-*cis*,15-*syn* configurations at a ratio of 3:1. The underlying photoreactions involve simultaneous isomerization of the C(13)=C(14) and C(15)=N bonds. Both isomers of this DA_{app} state may run through photoinduced reaction cycles initiated by photoisomerization of only the C(13)=C(14) bond. RR spectroscopic experiments further demonstrated that photoinduced conversion of the apparent dark-adapted (DA_{app}) state to the photocycle intermediates P500 and P390 is distinctly more efficient for the all-*trans* isomer than for the 13-*cis* isomer, possibly because of different chromophore−water interactions. Our data demonstrating two complementary photocycles of the DA_{app} isomers are fully consistent with the existence of two conducting states that vary in quantitative relation during light−dark adaptation, as suggested previously by electrical measurements.

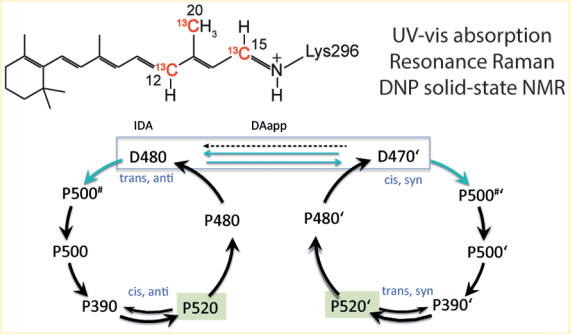

Channelrhodopsins (ChR) are microbial-type rhodopsins of motile unicellular algae that guide cells toward optimal light conditions. These photoreceptors function as light-gated channels with intrinsic conductance for $H^+ \gg Na^+ \sim K^+ > Ca^{2+}$. The underlying photoinduced processes allow several grades of adaptation within milliseconds in response to sudden light intensity changes over a wide dynamic range.[1,2] When longer light pulses are applied to ChR expressed in host cells, the initial peak current, I_p, decreases to a lower stationary current I_s in a process called "light adaptation".[3,4] At neutral extracellular pH (pH_e), the photocurrent recovers up to 70−80% after tens of seconds in darkness. We refer to this partially recovered state as the apparent dark-adapted state (DA_{app}). The original state with the maximal light sensitivity is named the initial dark-adapted (IDA) state. Full recovery of this IDA state takes much longer and is not complete even after 1 h.[3,4] Such a slow dark adaptation was originally shown for photocurrents of *Haematococcus pluvialis*.[5]

Light−dark adaptation and its effects on photocurrents depend on various parameters. At low pH_e, the reduction in photocurrents (or the ratio of peak to stationary current I_p/I_s) after light adaptation is lower and dark adaptation is faster.[3,6] Light−dark adaptation also depends on the membrane voltage. At a negative voltage, the effects on photocurrents are more significant than at a positive voltage. Further, during light adaptation, ion selectivity of the channel changes toward a higher selectivity for Ca^{2+}.[7] These observations could be explained only by the occurrence of two photocycles with distinct conducting states that are populated from two different dark states, as shown schematically in Figure 1. This concept is supported by the biexponential decay of the photocurrent, the ratio of which also depends on the pH gradient and membrane voltage.[3,7] This two-photocycle model sufficiently explained the kinetics of photocurrents under very different ionic and light conditions. On the basis of the similar UV−vis absorption of the all-*trans* and 13-*cis* dark states, we previously proposed that

Received: June 3, 2015
Revised: August 3, 2015
Published: August 3, 2015

DOI: 10.1021/acs.biochem.5b00597
Biochemistry 2015, 54, 5389−5400

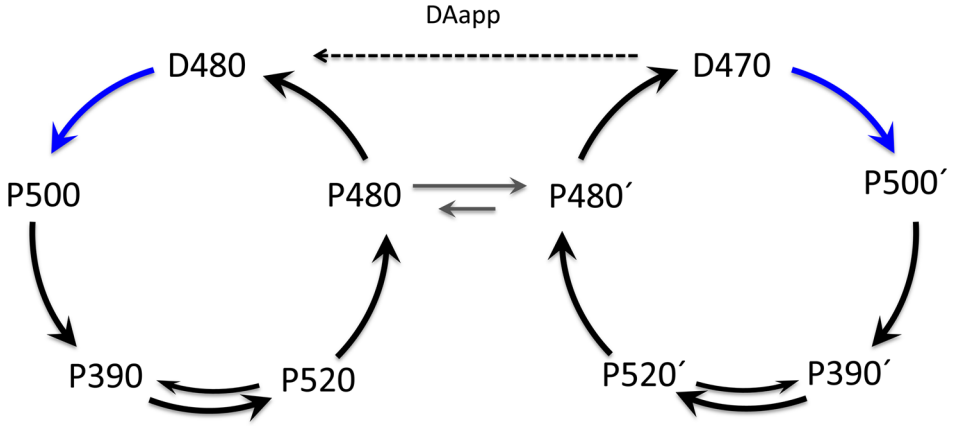

Figure 1. Simplified schematic of ChR-2 photocycles as established prior to this study.[9] Dark adaptation for several minutes following illumination leads to two parent states absorbing at 470 nm (D470) and 480 nm (D480), and the presence of only these two states is considered the "apparent dark-adapted state" (DA_{app}) from which two distinct photocycles are populated upon illumination (blue arrows). Thermal relaxation (black arrows) back to the dark states leads to the conversion into blue-shifted states containing a deprotonated Schiff base (P390 and P390′) and further into the conducting states (P520 and P520′). Both photocycles were assumed to be thermally connected via the late intermediates P480 and P480′. However, it remained a matter of debate whether and how fast D470 reconverts to D480 during extended dark periods (dashed arrow).

the 13-*cis* dark state includes the Schiff base in the 15-*syn* configuration in contrast to the 15-*anti* configuration of the corresponding all-*trans* state.[8,9]

However, the extent to which the two parent states of the photocycle model of Figure 1 thermally equilibrate in darkness remained a matter of debate. Retinal extraction and high-performance liquid chromatography (HPLC) analysis, as well as resonance Raman (RR) spectroscopic analysis in wild-type channelrhodopsin-2 (ChR2) and slow cycling mutants,[8−10] have revealed the existence of all-*trans* and 13-*cis* retinal isomers at ratios between 70:30 and 80:20 that obviously changed only very little during incubation of ChR in darkness. Thus, there is a need to identify precisely the changes in chromophore configuration associated with light−dark adaptation.

These objectives are the focus of this study, which is based on nuclear magnetic resonance (NMR) and optical spectroscopies. We investigated the IDA of detergent-solubilized ChR by solution NMR and of lipid-embedded protein by solid-state magic-angle spinning (MAS) techniques. Applying dynamic nuclear polarization (DNP) in conjunction with MAS NMR, we determined the retinal configuration. To investigate the composition of retinal isomers shortly after illumination (in DA_{app}), we applied RR spectroscopy using different temperatures and illumation protocols. The findings presented here will be discussed in the context of previously published electrophysiological data to relate the differential formation of conduction states to the reported effects of light adaptation on photocurrents.

EXPERIMENTAL PROCEDURES

Protein Expression and Purification. The ChR2-H134R and ChR2-C128S/D156A mutants were expressed, purified, and prepared in HEPES buffer (pH 7.4) according to previously described protocols.[11,12] Typical concentrations used for RR experiments corresponded to an optical density of 1−3 at 470 nm (OD_{470}). H/D exchange via buffered D_2O solution (pD 7.4) was achieved by dilution at 1:10 twice and subsequent protein concentration (Amicon ultra, 100000 molecular weight cutoff, Millipore, Temecula, CA).

The channelrhodopsin-1/channelrhodopsin-2 (C1C2) chimera construct 1−348[13,14] containing C-terminal different linker lengths and His tags was expressed in baculovirus/Sf9 insect cells and *Pichia pastoris*, resulting in proteins of 363 and 384 amino acids, respectively. The construct expressed in insect cells via the Bac-to-Bac baculovirus expression system was human codon-optimized and contained a TEV cleavage site. Sf9 cells were grown in suspension using Sf-900 II medium (Life Technologies, Carlsbad, CA) and infected with a 1:100 dilution of a high-titer virus stock at a density of 1.5×10^6 cells/mL for 72 h at 27 °C. C1C2-expressing cells were harvested by centrifugation for 10 min at 4000*g* and 4 °C, washed with buffer A [10 mM Tris (pH 7.4), 100 mM NaCl, 0.1 mM PMSF, and 1 mM EDTA] in the presence of 'cOmplete' protease inhibitors (Roche, Basel, Switzerland), and then stored at −80 °C. All subsequent steps were conducted at 4 °C. For incorporation of C(12)−C(15)−C(20)-^{13}C-labeled or unlabeled all-*trans* retinal into C1C2, thawed cells were resuspended in buffer B [20 mM Tris (pH 8.0), 100 mM NaCl, and 0.1 mM PMSF] and the chromophore was added to a final concentration of 88 μM. Then the cells were gently shaken for 16 h. Cells were then disintegrated, and C1C2-containing membranes were collected by ultracentrifugation, as described previously.[1,2] Protein solubilization was achieved by adding *n*-dodecyl β-D-maltoside (DDM, Glycon, Luckenwalde, Germany) and cholesterol hemisuccinate (CHS) to final concentrations of 2 and 0.5%, respectively. After incubation for 4 h, the sample was centrifuged (16000 rpm, 10 min), and protein in the supernatant was purified by Ni^{2+} affinity chromatography (5 mL-HIS trap FF crude column, GE Healthcare, Buckinghamshire, U.K.). After washing with 10 column volumes (CV) of buffer B supplemented with 50 mM imidazole and a 0.05% DDM/0.01% CHS mixture, C1C2 was eluted with buffer B with 500 mM imidazole and a 0.05% DDM/0.01% CHS mixture. The protein was desalted with a size-exclusion column (Hiprep 26/10 desalting, GE Healthcare) using buffer B with a 0.05% DDM/0.01% CHS mixture, concentrated as described above, and then stored at −80 °C.

For expression in *P. pastoris*, C1C2 (1−348) was cloned into pPIC (Life Technologies). Fermentation at a 1 L scale in a Fed Batch Pro System (Eppendorf, Hamburg, Germany) resulted in growth to an OD_{600} of 100 within 20 h at 30 °C. The culture was cooled to 20 °C, and a methanol-containing induction feed

DOI: 10.1021/acs.biochem.5b00597
Biochemistry 2015, 54, 5389−5400

was applied for 30 h, resulting in approximately 100 g of wet biomass. The cells were resuspended in a 10-fold volume of buffer C [20 mM Tris-HCl (pH 8.0) and 100 mM NaCl] containing 2 mM $MgCl_2$, EDTA-free cOmplete protease inhibitor mixture (Roche), Benzonase (5 units/mL, Merck, Kenilworth, NJ), and 10 μM C(12)−C(15)−C(20)-^{13}C-labeled retinal. The cells were then lysed, and membranes were collected as published previously.[1,2] Membrane proteins were solubilized with buffer C and 1% DDM, 20 mM imidazole, and 5 μM C(12)−C(15)−C(20)-^{13}C-labeled retinal at 8 °C overnight. The ultracentrifugation step was repeated, and the supernatant was applied to 2 mL of Ni-NTA (Qiagen, Limburg) equilibrated with buffer C containing 1% DDM and 20 mM imidazole at 8 °C overnight. After washing with buffer C supplemented with 50 mM imidazole and 0.03% DDM, C1C2 was eluted with buffer C with 500 mM imidazole and 0.03% DDM and then applied to a Sephacryl 300 column (110 mL) equilibrated with buffer C supplemented with 0.05% DDM.

Protein Reconstitution into Vesicles. Reconstitution of purified protein into lipid vesicles was conducted by detergent dialysis as described previously.[15] Briefly, Egg-PC (Avanti Polar Lipids Inc., Alabaster, AL) was mixed with concentrated protein to obtain a molar ratio of 100:1 or 80:1 (lipid:protein). The protein/vesicle mixture was then dialyzed against 1 L of buffer D [50 mM Tris (pH 7.5), 100 mM NaCl, 2 mM DTT, and 0.1 mM PMSF] or buffer E [20 mM HEPES (pH 7.5), 50 mM NaCl, and 1 mM $MgCl_2$] containing Amberlite XAD-2 adsorbent for 7 days at 8 °C in the dark. Buffer was exchanged every 24 h.

UV−Visible Absorption Spectroscopy. Absorption spectra were recorded at 20 and 0 °C using a Cary 50 Bio spectrophotometer (Varian, Inc., Darmstadt, Germany) at a spectral resolution of 1.6 nm. For low-temperature measurements, a Cary-1E UV/vis spectrophotometer was used. The cuvette was placed in a continuous flow helium cryostat (Oxford CF1204) or a variable-temperature liquid nitrogen bath cryostat (Oxford DN1704).[16] Samples including 65% (v/v) glycerol were illuminated with blue (455 nm, LEDC2, Thorlabs, Newton, NJ) or green (525 nm, LIU002, Thorlabs) LEDs.

RR Spectroscopic Measurements. RR spectra were measured with excitation lines of an Ar^+ (458, 514 nm) and Kr^+ laser (413 nm) (Coherent, Santa Clara, CA). The Raman signals were detected in a backscattering configuration (180°) via a confocal LabRamHR spectrometer (Horiba, Villeneuve, France), equipped with a liquid nitrogen-cooled CCD detector. Depending on the excitation line, the resolution per pixel was between 0.7 and 0.4 cm^{-1}, corresponding to a spectral resolution between 2.1 and 1.2 cm^{-1}. Typical accumulation times were 1 h with 0.1 mW at 298 K, 10 min with 10 mW at 298 K, and 1 h with 1 mW at 80 K. Further details of the setup and measurements are described elsewhere.[11]

Low-temperature experiments were conducted with a Linkam cryostat (Linkam Scientific Instruments, Surrey, U.K.) mounted on a computer-controlled XY stage (OWIS GmbH). The cryostat was circularly moved to avoid heating of the sample surface in the laser focus. The samples were inserted into the cell under dimmed red light to prevent photoactivation before freezing.

Single-beam time-resolved RR measurements at ambient temperature were performed using the rotating cell and magnetic mixing ball technique.[17,18] This approach allows for controlling the sample composition in the laser beam via the photoconversion parameter $\Delta t_{las} I_0$, where Δt_{las} is the residence time of the sample in the laser beam and I_0 depends on laser power P_{las} and the photophysical parameters of ChR. In our experiments, Δt_{las} was adjusted to ∼30 μs such that when 458 nm excitation and a laser power of 0.1 mW were applied, a photoconversion during Δt_{las} of <5% was estimated. The correct choice of excitation parameters was verified by further reduction of the laser power that did not alter the spectrum. Alternatively, higher laser powers (10 mW) were used to initiate photoconversion during the RR probe event and thus to probe photocycle intermediates generated during the residence time of the sample in the laser beam. In both the "low-power" and "high-power" experiments, effective mixing of the irradiated volume with an ∼10^5-fold larger reservoir makes multiple excitations highly unlikely during the typical accumulation time of approximately 1 h (see the Supporting Information for details).[17] In all spectra shown in this report, the background was subtracted by a polynomial function. Band fitting and component analysis were conducted as described previously.[19,20]

NMR Spectroscopy. ^{1}H−^{13}C correlation spectra[21] in solution were recorded at 298 K using samples of 7.5 and 6.0 mg of C1C2 in a 0.05% DDM/0.01% CHS mixture, reconstituted upon purification from insect cells with C(12)−C(15)−C(20)-^{13}C-labeled all-*trans* and unlabeled retinal, respectively. The spectra of the labeled sample were recorded on a 900 MHz Avance spectrometer (Bruker, Billerica, MA), while the reference spectra were recorded on a 600 MHz Avance spectrometer. Both were equipped with a 5 mm Cryoprobe. Several spectra were recorded in two ways, with the transmitter frequency either at 50 ppm or at 150 ppm, to optimize decoupling performance. Acquisition times were 10.2 and 68.2 ms in t_1 and t_2, respectively.

Solid-state magic-angle spinning (MAS) NMR spectra were acquired using 4.7 mg of C1C2 expressed in *P. pastoris* and reconstituted with C(12)−C(15)−C(20)-^{13}C-labeled all-*trans* retinal. The protein was integrated into vesicles at a molar ratio of 100:1 (lipid:protein) as described above. Two-dimensional (2D) ^{13}C−^{13}C correlation spectra at 266 K were recorded using the dipolar-assisted rotational resonance (DARR)[22] mixing scheme on a 800 MHz Avance wide-bore spectrometer (Bruker) equipped with a triple-resonance (^{1}H/^{13}C/^{15}N) 3.2 mm MAS Efree probe (Bruker). The MAS frequency was adjusted to 17777 Hz. A linear ramp (from 75 to 100%) was applied during ^{1}H cross-polarization (CP)[23,24] and a recycle delay of 3 s to avoid sample heating. ^{1}H decoupling was achieved with SPINAL-64[25] during evolution and acquisition, applying a radiofrequency strength of 75 kHz. Acquisition times were 27.7 and 3.2 ms in t_2 and t_1, respectively.

Dynamic nuclear polarization (DNP) spectra were recorded at 100 K and a MAS frequency of 8889 Hz on a 400 MHz Avance wide-bore spectrometer (Bruker) equipped with a triple-resonance (^{1}H/^{13}C/^{15}N) 3.2 mm MAS DNP probe and a 264 GHz gyrotron as a microwave source, using the same sample as described above after transfer into a buffer containing 60% (v/v) glycerol-d_8, 30% (v/v) D_2O, 10% (v/v) H_2O, and 20 mM biradical TOTAPOL.[26] 2D ^{13}C−^{13}C correlation spectra were recorded with the DARR mixing scheme. Similar conditions for initial polarization transfer and ^{1}H decoupling were chosen to be analogous to those of the measurements at 800 MHz with acquisition times of 19.9 and 2.0 ms in t_2 and t_1, respectively.

DOI: 10.1021/acs.biochem.5b00597
Biochemistry 2015, 54, 5389−5400

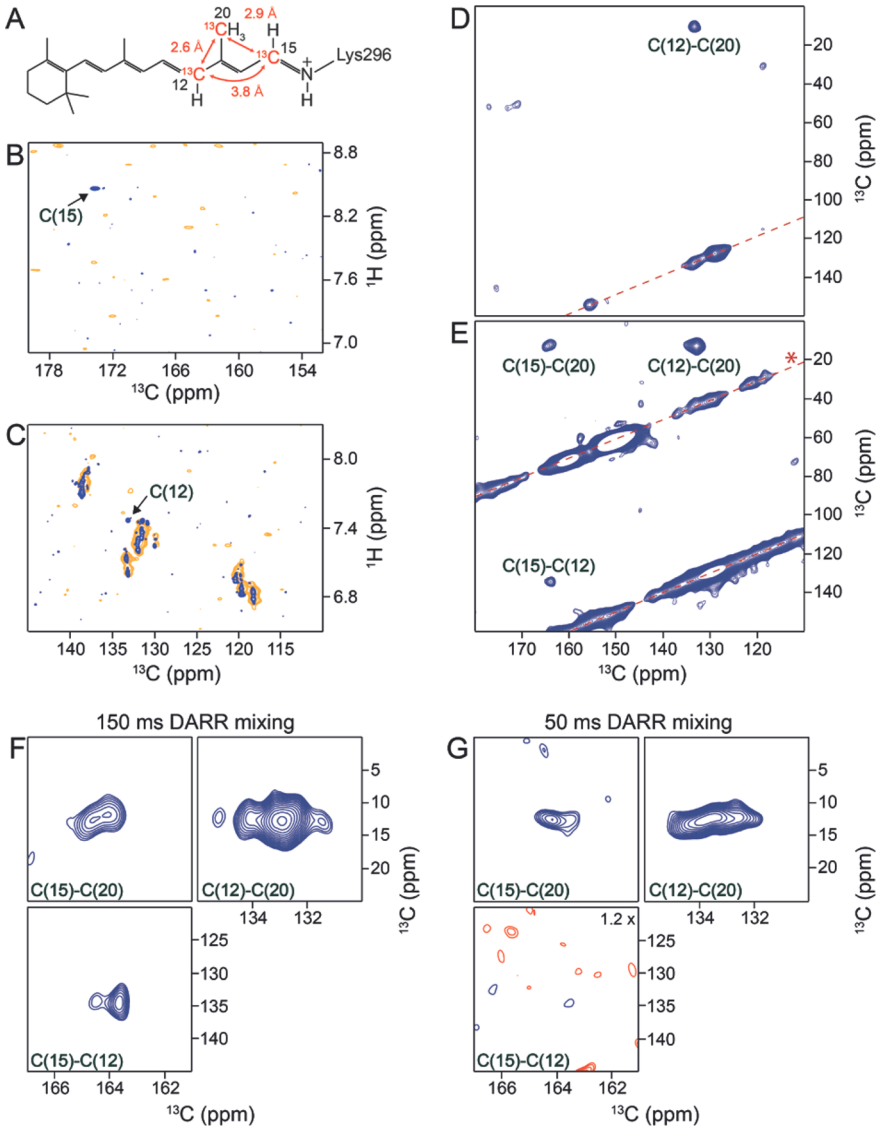

Figure 2. Solution and solid-state NMR spectra of retinal bound to the ChR chimera C1C2 in the IDA state. (A) ^{13}C labeling scheme of the retinal. (B and C) Enlarged regions of the C(15) and C(12) chemical shifts in the 2D ^{13}C−^{1}H heteronuclear multiple-quantum correlation (HMQC) solution NMR spectra recorded at 298 K. The protein was solubilized in detergent (pH 7.4). The spectra of C1C2, including an unlabeled and ^{13}C-labeled retinal, are colored orange and blue, respectively. (D) 2D ^{13}C−^{13}C DARR solid-state NMR spectrum (T = 266 K) recorded with a mixing time of 150 ms and a MAS frequency of 17777 Hz. A red dashed line indicates the main diagonal. (E) DNP-enhanced 2D ^{13}C−^{13}C DARR solid-state NMR spectrum (T = 100 K) with a mixing time of 150 ms and a MAS frequency of 8889 Hz. Red dashed lines indicate the main diagonal and the spinning sideband (marked with a red asterisk). (F and G) Enlarged sections of C(15)−C(20), C(12)−C(20), and C(15)−C(12) cross-peaks of DNP-enhanced 2D ^{13}C−^{13}C DARR solid-state NMR spectra with processing parameters for high resolution. DARR mixing times of 150 ms (F) and 50 ms (G, for detection of short-range distances) were used. An enlarged region of the missing C(15)−C(12) cross-peak in panel G is plotted vs noise by a factor of 1.2. Negative (red) and positive (blue) contours are shown. The spectra in panels D and E refer to C1C2 (including ^{13}C-labeled retinal) reconstituted in liposomes.

All solid-state NMR spectra were referenced using the downfield signal (40.48 ppm) of adamantane as an external standard. Solution NMR spectra were externally referenced using 4,4-dimethyl-4-silapentane-1-sulfonic acid (DSS). All NMR data were processed with TOPSPIN 3.2 (Bruker) by using appropriate window functions and baseline correction after Fourier transformation.

RESULTS

Examination of the IDA State by NMR Spectroscopy. We first analyzed the configuration of retinal isomers potentially appearing in the IDA, i.e., the state that is formed after dark adaptation within hours. To this end, we performed NMR spectroscopy on the channelrhodopsin-1/channelrhodopsin-2 (C1C2) chimera[13,14] after it had been kept in the dark for >1.5 h prior to the start of the experiment. Two types of samples were investigated, detergent-solubilized for solution NMR measurements, and embedded into lipid vesicles for solid-state MAS NMR measurements. In both cases, the protein was reconstituted with C(12)−C(15)−C(20)-^{13}C-labeled retinal (Figure 2A) after cells had been harvested. This reconstitution procedure was less efficient with ChR2 that has been used for most electrophysiological and spectroscopic studies. Hence, all NMR experiments were conducted with C1C2. Depending on the presence of a 13-*cis* or 13-*trans* double bond, the chosen labeling pattern allowed for the

DOI: 10.1021/acs.biochem.5b00597
Biochemistry 2015, 54, 5389−5400

detection of cross-peaks between C(15) and C(12) relative to C(20) that were sized in proportion to the respective distances.

The solution NMR spectra indicate the presence of only one isomer in the IDA state (Figure 2B,C). In particular, one sharp, well-shaped cross-peak for the C(15)-H moiety was detected at ^{13}C and ^{1}H chemical shifts of 173.7 and 8.5 ppm, respectively (Figure 2B). We did not observe any overlap with a second peak at similar frequencies, which could potentially occur because of the presence of a 13-*cis*,15-*syn* conformer. In general, cross-peaks from a second retinal in a *cis* configuration are expected to be shifted downfield in the ^{13}C and ^{1}H dimensions for both the 15-*syn* and 15-*anti* configurations.[27] As expected, no signal occurred in the C(15) area of the spectrum recorded from the unlabeled reference sample (Figure 2B, orange). The cross-peak of the C(12)-H moiety appeared at ^{13}C and ^{1}H chemical shifts of 133.0 and 7.5 ppm, respectively (Figure 2C).

To determine the configuration of the bond between C(13) and C(14) in the C1C2 form constituting the IDA state, $^{13}C-^{13}C$ correlations were then recorded from protein samples that were reconstituted into lipid vesicles, using the dipolar-assisted rotational resonance (DARR) technique (Figure 2D). The cross-peak found at ^{13}C chemical shifts of 133.3 and 10.5 ppm indicates a through-space interaction between C(12) and C(20) of the retinal. However, the cross-peaks expected at around 170 and 130 ppm in F_2 and F_1 [for the $^{13}C(15)-^{13}C$-(12) interaction] and 170 and 10 ppm in F_2 and F_1 [for the $^{13}C(15)-^{13}C(20)$ interaction], respectively, were not observed at the signal-to-noise (S/N) level achieved in 10 days.

To improve the S/N level by at least 1 order of magnitude, we applied DNP MAS NMR at 100 K. Next to the gain by DNP, higher cross-polarization (CP) transfer rates are obtained because of the low temperatures that rigidify the membrane. The $^{13}C-^{13}C$ correlations recorded under DNP conditions showed the expected cross-peak pattern (Figure 2E−G). The cross-peak for the $^{13}C(15)-^{13}C(12)$ through-space interaction appeared in this spectrum at ^{13}C chemical shifts of 164.4 and 133.5 ppm in F_2 and F_1, respectively, whereas the ^{13}C-(15)$-^{13}C(20)$ interaction produced a cross-peak at ^{13}C chemical shifts of 164.4 and 12.6 ppm in F_2 and F_1, respectively (Figure 2E). Optimizing the processing parameters resulted in enhanced resolution, which then revealed that the seemingly "pure" cross-peaks were composed of at least two components (Figure 2F), as expected with low-temperature NMR spectroscopy.[28]

To ensure that the observed proportionality of cross-peak intensities reflected the differences in internuclear distances, a spectrum with a short mixing time of 50 ms was also recorded (Figure 2G). The spectrum indeed shows the expected intense cross-peak(s) involving C(15) and C(20) and no signal connecting C(12) and C(15). This is valid for all components of the cross-peak assemblies involving C(15), indicating a 13-*trans* configuration of the retinal in all cases. Conclusions concerning the status of the double bond between the lysine nitrogen and C(15) of the retinal cannot be made at this point with the labeling pattern chosen for this study.

RR Spectroscopic Assessment of the DA_{app} State at Ambient Temperature. Next, we performed RR spectroscopy to examine the composition of the retinal isomers in the wild-type (WT)-like ChR2-H134R variant ChR following dark adaptation for several minutes, DA_{app}. The spectra were recorded at ambient temperature with a low laser power of 0.1 mW at 413, 458, and 514 nm excitation using the rotating cell technique (see Experimental Procedures) (Figures 3 and 4). The excitation conditions were chosen so that the photoconversion during the sample residence time in the exciting laser beam would be less than 5% (Figure 3A and Figure 4, left panel).

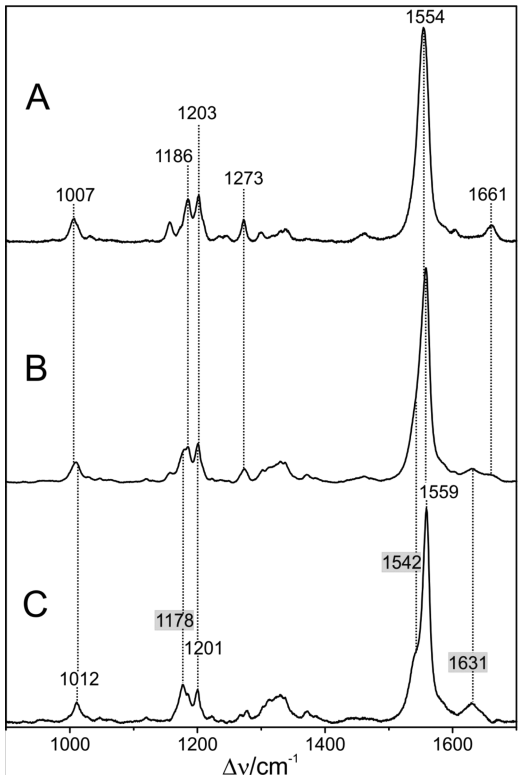

Figure 3. RR spectra of ChR2-H134K measured at 298 K with 458 nm excitation at different laser powers: (A) P = 0.1 mW, and (B) P = 10 mW. (C) Difference spectrum obtained by subtracting spectrum A from spectrum B. The spectra were obtained from samples in H_2O at pH 7.4.

In addition, efficient stirring of the samples via the magnetic ball technique ensured "fresh sample" conditions at the entry point of the laser beam. Because of the large sample reservoir in the cuvette, the probability that proteins were irradiated a second time during the entire time spectra were being recorded (~1 h) was negligibly small (see the Supporting Information). Under these conditions, the low-power experiments primarily probe the DA_{app} state, including a potential mixture of all-*trans* and 13-*cis* chromophores, representing the parent state of the two photocycles (Figure 1). In addition, in the sample reservoir, a slow thermal conversion from the DA_{app} to IDA state was expected to occur during spectrum accumulation (*vide infra*).

The relative contributions of the two putative all-*trans* and 13-*cis* retinal isomers were determined using a previously published procedure.[19] Accordingly, it was assumed that the C═C stretching modes in both isomers include two components of strong and weak RR intensity, representing the two isomers.[29,30] The three RR spectra in Figure 4 (left panel) were analyzed with a global fitting procedure using the peak intensities as freely adjustable parameters, because only their relative intensities could be affected by the excitation wavelength. This analysis produced the component spectra of the all-*trans* and 13-*cis* isomers with the in-phase C═C

DOI: 10.1021/acs.biochem.5b00597
Biochemistry 2015, 54, 5389−5400

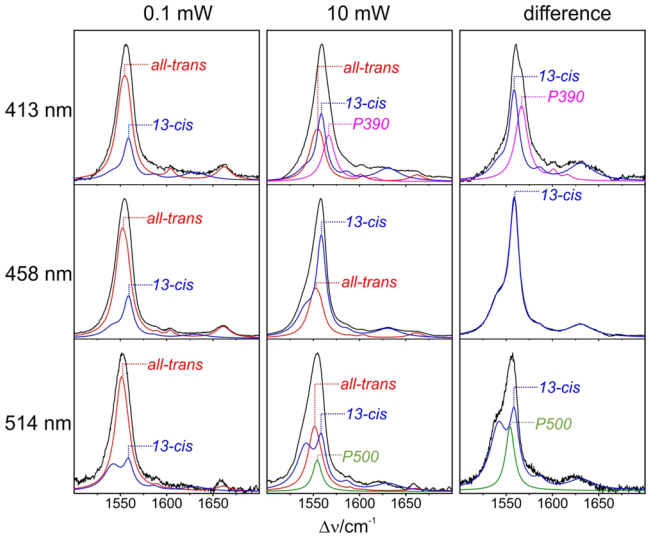

Figure 4. RR spectra of ChR2-H134K measured at 298 K with different excitation lines (indicated on the left side) and different laser powers (top labels; P = 0.1 mW, and P = 10 mW). The right panel shows the difference spectra ("10 mW" minus "0.1 mW") at the respective excitation lines. The spectra, which were obtained from samples in H_2O at pH 7.4, show the C=C and C=N stretching region, including the results of band fitting analysis. The solid red and blue lines represent the component spectra of the all-*trans* and 13-*cis* chromophores, respectively. The component spectra of the photocycle intermediates P390 (detectable at 413 nm) and P500 (detectable at 514 nm) are displayed as solid magenta and green lines, respectively. The individual peak positions are listed in Table S2.

stretching modes at 1551.0 and 1558.7 cm^{-1}, respectively (Table S2). These frequencies indicate a slightly red-shifted absorption maximum (λ_{max}) for the all-*trans* form compared to the 13-*cis* form according to the inverse $\nu_{C=C}/\lambda_{max}$ relationship.[31] Assuming similar RR cross sections for the strongest (in-phase) C=C stretching modes of the two isomers, the all-*trans*:13-*cis* ratio was 75:25, which is within the range of previously published values for the DA_{app} state of ChR2.[8−10] This result is in contrast to the IDA state, which solely contains the all-*trans* form as revealed by NMR (*vide supra*). The same analysis was applied to RR spectra measured from samples in D_2O (pD 7.4) under otherwise identical conditions (Table S2). Furthermore, results essentially the same as those with ChR2 were obtained for the C1C2 variant of ChR (Figure S2). Taken together, we obtained spectra showing two retinal isomers in all cases assessed.

Photoconversion of the Apparent DA_{app} State. To further study photoconversion of the two isomers in DA_{app}, we measured RR spectra at ambient temperature using a high laser power (10 mW) under otherwise identical conditions [$\Delta t_{las} \approx$ 30 μs (Figure 3B and Figure 4, middle panel)]. Because the residence time of the sample in the laser beam was within the range of the P500 decay time and the P390 rise time (Table S1), these two intermediates accumulated at the expense of the DA_{app} state while later photocycle intermediates remained undetected (Figure 4, middle panel). However, the amount of photoconversion along with the resonance enhancements of the dark states and photocycle intermediates varied with the three excitation wavelengths. At 458 nm excitation, the parent DA_{app} state was preferentially enhanced and the intermediates remained invisible. At 514 and 413 nm excitation, the spectral weights of P500 and P390 were increased, respectively. The low-power spectrum of the parent DA_{app} state was subtracted from the high-power spectrum for each wavelength, so that negative signals were avoided (Figure 4, right panel). The resultant spectra reflected the formation of photocycle intermediates and changes in the isomeric composition of the parent DA_{app} state. The high-power spectrum recorded at 458 nm excitation, which impaired detection of the two

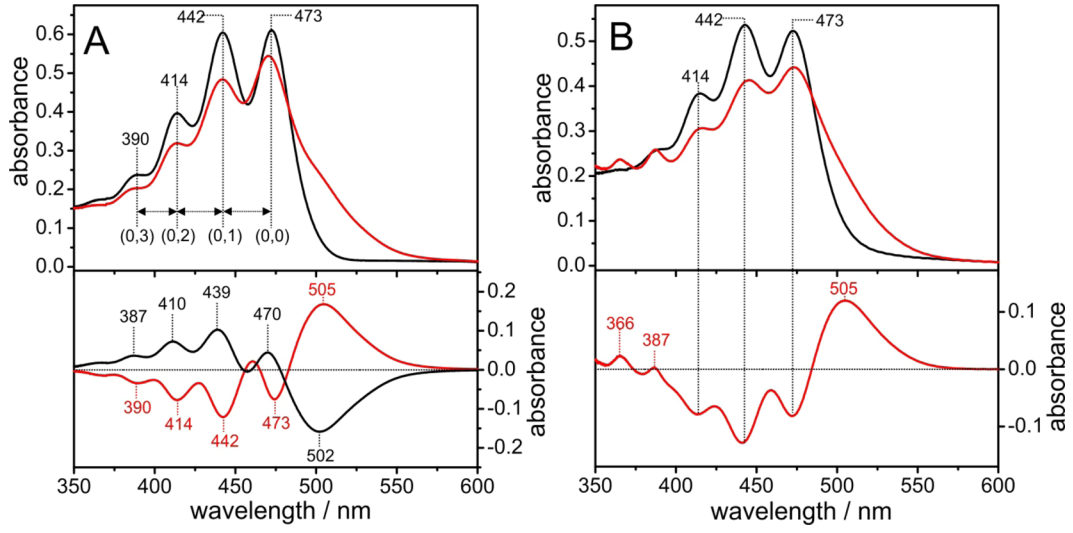

Figure 5. (A) Absorption spectra (top) of ChR2-H134R measured at 4 K in the DA_{app} state before (black line) and after (red line) blue-light irradiation (455 nm) at 4 K. The vertical dotted lines mark the vibronically resolved bands with a progression of approximately 1500 cm^{-1} corresponding to the C=C stretching mode of the retinal chromophore. The spectra were obtained from frozen samples in H_2O at pH 7.4. Resultant difference spectrum (bottom) after subtracting the "before irradiation" spectrum from the "after irradiation" spectrum (red line). The black line represents the reverse process, i.e., the difference spectrum after the additional irradiation with green light (525 nm) at 4 K. (B) Absorption spectra (top) of ChR2-H134R measured at 80 K in the DA_{app} state before (black line) and after (red line) blue-light irradiation at 220 K and measured at 80 K. The spectra were obtained from frozen samples in H_2O at pH 7.4. Difference spectrum (bottom) obtained as described for panel A.

DOI: 10.1021/acs.biochem.5b00597
Biochemistry 2015, 54, 5389−5400

intermediates, revealed that the magnitude of the 13-*cis* isomer component of the DA_{app} state was significantly increased at the expense of the all-*trans* isomer. At 413 nm excitation, an additional band at 1567 cm^{-1} was detected, which we attributed to P390. Its frequency was assigned to that of the C=C stretching vibration of deprotonated retinal Schiff bases (RSBs).[11,32,33] Similarly, the extra band at 1554 cm^{-1} in the 514 nm spectrum was assigned to the P500 intermediate. Altogether, we conclude that, at ambient temperature, the photoconversion of DA_{app} at higher light intensities leads to the production of photocycle intermediates accompanied by preferential depletion of the all-*trans* retinal isomer and accumulation of the 13-*cis* form.

ChR Photoreactivity at Low Temperatures. Photoconversion of the DA_{app} state was further analyzed at low temperatures to block thermal relaxation processes of different intermediates of the photocycle. The UV−vis absorption spectrum of the parent DA_{app} state of ChR2-H134R, measured at 4 K, displays a vibronic fine structure with peaks at 473, 442, 414, and 390 nm (Figure 5A). The spacing between the various peaks was approximately 1500 cm^{-1}, corresponding to the C=C stretching mode of the retinal. Irradiation with blue light (455 nm) eliminated the DA_{app} bands and yielded a new absorption at approximately 505 nm, indicating photoisomerization of a fraction of the chromophores and transition into the first photocycle intermediate, P500.[34,35] The process could be reversed upon irradiation with green light (525 nm). The underlying retinal isomerization did not have any significant thermal activation barrier. Examinations at 80 K (Figure 5B), the temperature at which RR spectroscopic measurements were conducted, led to essentially the same UV−vis spectra and response to blue irradiation.

Next, RR spectra were measured at 80 K with 413, 458, and 514 nm excitation (Figure 6). The analysis was guided by the RR component spectra of the all-*trans* and 13-*cis* isomers obtained at ambient temperature while taking into account the typical frequency upshifts and band narrowing at low temperatures.[20] Remarkably, the RR spectra at all three wavelengths were very similar and, in contrast to the UV−vis spectra, do not display any contribution from the P500 intermediate expected at approximately 1550 cm^{-1}. This discrepancy can readily be attributed to the weak resonance enhancement at 468 and 413 nm (*vide supra*). The failure to detect P500 in the spectra measured with 514 nm excitation, however, can be explained only by a low enrichment of P500 in the photostationary mixture because of the more efficient back reaction at this wavelength.

When the temperature was increased to 220 K, blue irradiation (455 nm) caused the appearance of two small additional bands at 387 and 366 nm in the UV−vis spectra (Figure 5B, spectra measured at 80 K after irradiation at 220 K) due to the accumulation of P390 in addition to the P500 species. The analogous RR experiment (i.e., after blue-light irradiation at 220 K) now shows contributions from both the P390 and P500 intermediates at 413 and 514 nm excitation, respectively (Figure 6). This finding implies that the P500 states formed at 80 and 220 K are not identical even though the optical spectra are essentially the same. We therefore conclude that the transition to the P500 intermediate, generated at 220 K, is associated with relaxation of the protein environment surrounding the chromophore that impairs a photochemical back reaction of the P500 intermediate, obtained at 80 K, to the DA_{app} state. By translating the temperature scale to the time

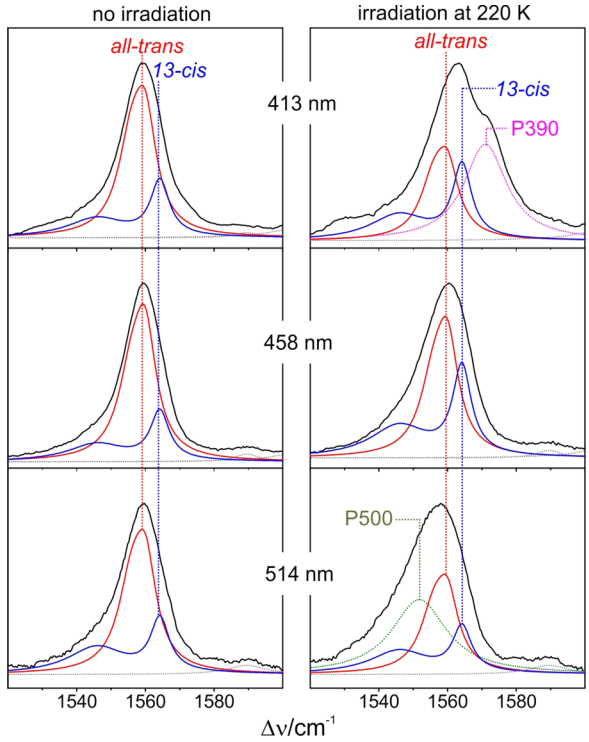

Figure 6. RR spectra of ChR2-H134R measured at 80 K with different excitation lines (P = 1 mW) without additional irradiation (left) and after blue-light irradiation (455 nm) at 220 K (right). The spectra, which were obtained from samples in H_2O at pH 7.4, show the C=C stretching region, including the results from band fitting analysis. The solid red and blue lines represent the component spectra of the all-*trans* and 13-*cis* chromophores, respectively. The component spectra of the photocycle intermediates P390 (detectable at 413 nm) and P500 (detectable at 514 nm) are displayed as dotted magenta and green lines, respectively.

scale, we denote the P500 species at 80 and 220 K as "early" and "late" P500, respectively.

Determination of the C=N Schiff Base Conformations in the DA_{app} State. To determine the conformation of the C=N bond, we re-examined the RR spectra obtained at ambient temperature with 458 nm excitation at low and high laser powers (Figure 3). These spectra display the all-*trans* and 13-*cis* isomers occurring in DA_{app} exclusively, albeit at different ratios such that appropriate linear combinations could resolve the pure spectra of the two isomers. The required weighting factors were readily evaluated from the component analysis of the C=C stretching region (Figure 4). This procedure, which was also extended to the spectra measured in D_2O, did not produce negative bands (Figure 7), providing further support for the effectiveness of the component analysis.

For the all-*trans* isomer of the DA_{app} state in H_2O and D_2O, we observed far-reaching spectral similarities with the parent state of light-adapted bacteriorhodopsin (BR_{LA}), indicating an all-*trans*,15-*anti* RSB geometry.[36] However, notable differences were found in the Schiff base stretching mode of unusually high frequency, which was 1661.1 cm^{-1} (Figure 7A) compared to 1641 cm^{-1} in BR_{LA}. In D_2O, this mode was observed at a typical frequency of 1631.8 cm^{-1} (Figure 7B), which is similar to that of protein-bound protonated RSBs in other microbial rhodopsins (e.g., 1626 cm^{-1} in BR_{LA}).[36] Both the high frequency and the large H/D isotopic shift can be related to specific coupling of the N−H in-plane (ip) bending and the

DOI: 10.1021/acs.biochem.5b00597
Biochemistry 2015, 54, 5389−5400

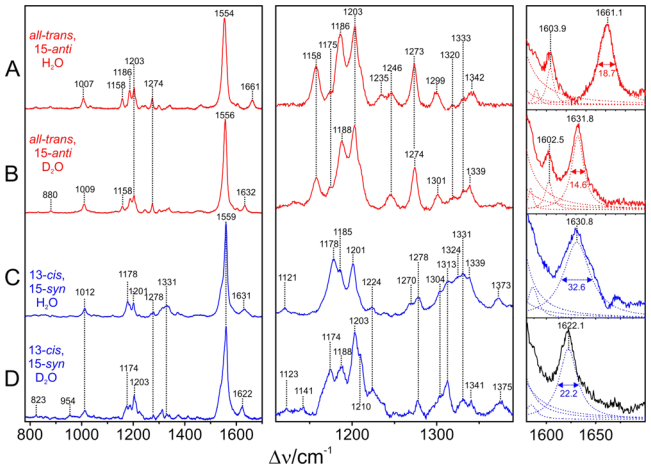

Figure 7. RR spectra of the two isomers of the light-adapted state of ChR2-H134K: (A) all-*trans*,15-*anti*/H_2O (red), (B) all-*trans*,15-*anti*/D_2O (red), (C) 13-*cis*,15-*syn*/H_2O (blue), and (D) 13-*cis*,15-*syn*/D_2O (blue). The spectra were obtained by weighted subtraction of the spectra measured at 458 nm with low and high laser power. The weighting factors were derived from component analysis in the C=C and C=N stretching region as shown for the sample in H_2O (pH 7.4) in Figure 4. The spectra of the chromophores deuterated at the Schiff base nitrogen were obtained in the same way from samples in D_2O (pD 7.4). The left and middle panels show the overview spectra and the fingerprint region on an enlarged scale, respectively. Band fitting analysis of the C=N stretching region is shown in the right panel. Blue and right-hand numbers indicate the bandwidths (in cm^{-1}) of the $C{=}NH^+/C{=}ND^+$ stretching modes.

C=N stretching coordinates. Increased coupling was suggested to shift the $C{=}NH^+$ stretching to higher frequencies, thereby increasing the H/D isotopic shift due to removal of this coupling in D_2O.[36] The origin of such increased coupling may result from stronger hydrogen bonding interactions, which in turn cause a downshift in the mode of predominantly N−H ip bending.[37] This interpretation is in fact supported by the unusually low frequency of this mode, which is assigned to the band at 1235 cm^{-1} (Figure 7A). There is essentially no coupling of the N−H ip coordinate with C−H ip and C−C stretching coordinates because no further notable H/D isotopic shifts were observed within the fingerprint region between 1100 and 1400 cm^{-1}. This behavior is characteristic of an *anti* conformation of the Schiff base as demonstrated by comparison of the RR spectra of BR_{LA} (all-*trans*,15-*anti*) and the 13-*cis*,15-*anti* intermediates K590 and L550 of BR.[36,18] Therefore, these findings confirm that the all-*trans* isomer in the DA_{app} state of ChR2 exists in the all-*trans*,15-*anti* configuration.

The 13-*cis* chromophore of the DA_{app} state displayed a significantly lower C=N stretching frequency (1630.8 cm^{-1}) and a much smaller H/D isotopic downshift [8.7 cm^{-1} (Figure 7C,D)] compared to those of the all-*trans* chromophore. This cannot be explained in terms of weaker hydrogen bond interactions. Instead, this phenomenon can be attributed to a different coupling scheme by the N−H ip coordinate because of the *syn* conformation of the Schiff base. In this conformation, the N−H ip coordinate couples with C(14)−C(15) stretching and the C(15)−H ip coordinates as shown for the 13-*cis*,15-*syn* RSB component of dark-adapted BR (BR_{DA}).[38] Because these couplings are eliminated under D_2O conditions, more modes are affected by D_2O in the Schiff base *syn* conformation than in the *anti* conformation. This was in fact observed in the spectra of the 13-*cis* retinal species of the DA_{app} state, which displays substantial H/D isotopic effects within the fingerprint region (Figure 7C,D). These include the bands at 1178, 1185, and 1324 cm^{-1}, which presumably involve the C(14)−C(15) and C(15)−H ip coordinates.[38] The largest N−H ip contribution was attributed to the band at 1270 cm^{-1}, which is consistent with assigning the 954 cm^{-1} band to a largely pure N−D ip mode in the DA_{app}-state spectrum in D_2O. Taken together with the far-reaching spectral similarities of the corresponding isomer of BR_{DA},[38] the 13-*cis* RSB component of the DA_{app} state adopts a 13-*cis*,15-*syn* configuration.

Assessment of Vibrational Energy Transfer of the Schiff Base. For both isomers of the DA_{app} state, changes in the bandwidths of the $C{=}NH^+$ stretching modes (1622−1662 cm^{-1}) were observed upon H/D exchange. This effect, which has been reported previously in BR_{LA}[39] and ChR,[10] was analyzed separately in the all-*trans* and 13-*cis* chromophores. As in the case of BR_{LA}, the line broadening of the $C{=}NH^+$ stretching modes (Figure 7A,C, right panel), which is particularly pronounced for the 13-*cis*,15-*syn* isomer, could be the result of changes in the lifetime of vibrationally excited states as a consequence of vibrational energy transfer to an energetically similar bending mode (approximately 1635 cm^{-1}) of a nearby H_2O molecule. Such an energy transfer is not possible for the $C{=}ND^+$ stretching mode as the corresponding D_2O bending mode (approximately 1200 cm^{-1}) does not fulfill the energy resonance conditions. Thus, the bandwidths of the $C{=}NH^+$ and $C{=}ND^+$ stretching modes can be used to determine vibrational lifetimes in the presence and absence of vibrational energy transfer, thereby allowing estimation of the rate constants for energy transfer from the RSB to adjacent water molecules for the two isomers (see the Supporting Information for further details). Assuming a Förster-type mechanism for the collision-less intermolecular energy transfer,[40] the different values for the all-*trans* and 13-*cis* chromophores should primarily be due to different distances R_{trans} and R_{cis} between the water molecule and the Schiff base. Thus, we obtain $R_{trans} = 1.17R_{cis}$ (Table S3).

Determination of the Chromophore Configurations in P390. To probe the RR spectrum of the P390 state, we used the slow-cycling ChR2-C128S/D156A variant, which, after photoexcitation, resides in the P390−P520 equilibrium for >1 h with a major contribution from P390 (Figure S1).[41]

We first measured the RR spectra of the parent DA_{app} state of ChR2-C128S/D156A at ambient temperature with 458 nm excitation. This dark spectrum is consistent with that of DA_{app} in ChR2 except for a slightly higher 13-*cis* content in the slow-cycling mutant (Figure S3). Note that despite continuous mixing of the irradiated volume within the large sample reservoir, the "fresh-sample" condition was most likely not fully established because of the long lifetime of the P390 intermediate. However, there is no detectable contribution of this species in the RR spectrum because of weak resonance enhancement at 458 nm.

Conversely, a pure RR spectrum of P390 could be obtained upon 413 nm excitation by weighted subtraction of a spectrum acquired with a low laser power (0.1 mW; small P390 contribution) from that measured with a high laser power (10 mW; large P390 contribution) (Figure 8A). This spectrum revealed the characteristic signature of a deprotonated RSB, including the lack of isotopic shifts upon H/D exchange and a high frequency of C=C stretching at approximately 1570 cm^{-1}. We also found some striking spectral differences compared to the M410 state of BR_{LA} (Figure 8B), in which

DOI: 10.1021/acs.biochem.5b00597
Biochemistry 2015, 54, 5389−5400

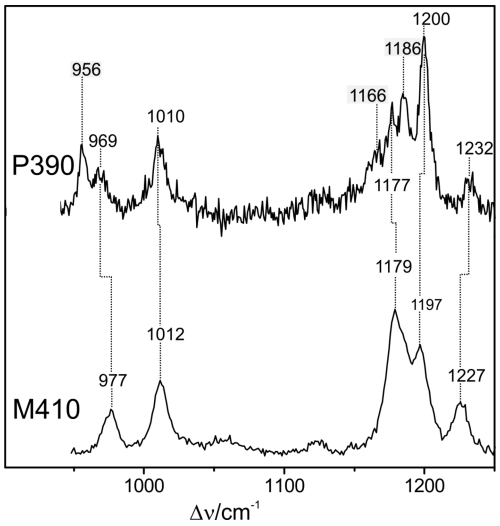

Figure 8. RR spectra of the UV-absorbing intermediates P390 of ChR2-C128S/D156A and M410 of BR. The top spectrum is the P390 spectrum obtained by subtracting the low-power spectrum (0.1 mW) from the high-power spectrum (10 mW) to remove contributions of the parent DA_{app} state. The spectra were measured with 413 nm excitation from a sample in H_2O (pH 7.4) at 298 K. The bottom spectrum is the the M410 spectrum taken from ref 11.

the deprotonated RSB adopts an exclusively 13-*cis*,15-*anti* configuration. First, the spectrum of ChR2-C128S/D156A P390 exhibits a larger number of bands within the fingerprint region between 1100 and 1250 cm^{-1}. Moreover, its intensity pattern differs substantially from that of the M410 state, suggesting an isomeric heterogeneity in the chromophore at the P390 state. In fact, whereas for the deprotonated 13-*cis* RSB the C(14)−C(15) stretching mode at approximately 1175 cm^{-1} exhibits a RR activity higher than that of the C(8)−C(9) stretching mode at approximately 1200 cm^{-1},[33] the intensity ratio is reversed in deprotonated all-*trans* RSB.[42] Thus, the band pattern within the fingerprint region of the P390 state may be explained in terms of overlapping contributions from deprotonated all-*trans* and 13-*cis* RSBs. Consistent with this interpretation are the spectral changes in the C−H out-of-plane deformation (HOOP) region below 1000 cm^{-1}. For an all-*trans* RSB, the HOOP mode of the C(11)−C(12) entity gains RR intensity compared to that of 13-*cis* RSB.[33,42] Accordingly, we assigned the bands at 956 and 969 cm^{-1} to the respective HOOP modes of the all-*trans* and 13-*cis* deprotonated RSB isomers, respectively. We thus conclude that, unlike the pure 13-*cis*,15-*anti* configurations of the chromophore in M410 of BR, the P390 state of ChR2 includes deprotonated RSBs in both all-*trans* and 13-*cis* configurations.

DISCUSSION

The Initial Dark State and the Apparent Dark-Adapted State. The crystal structure of the C1C2[14] chimera demonstrates that the retinal chromophore adopts an all-*trans*,15-*anti* configuration. However, on the basis of the electron density map, a contribution from a 13-*cis* retinal cannot be excluded.[14] A uniform retinal structure[43] is contradicted by the results from several spectroscopic studies of numerous ChR2 variants, which revealed isomeric mixtures of retinal chromophores in line with retinal extraction experiments.[8−10] We know from previous experiments that the ChR DA_{app} state, as reached within 1 min in darkness, depends on the history of illumination and, in particular, on the applied wavelength. For ChR2, illumination with blue light (470 nm) or green light (520 nm) resulted in apparent dark states called the dark-adapted state after green illumination (DAG) and dark-adapted state after blue illumination (DAB). The relative composition of all-*trans* and 13-*cis* retinal differs between these two states, with ratios of 60:40 and 80:20 observed for DAG and DAB, respectively.[9] The NMR experiments presented here unequivocally prove that the fully dark-adapted state (IDA) of ChR consists of protein that contains only all-*trans* retinal. This state is likely to be identical to the IDA previously postulated for newly synthesized ChR.[9,44,45] It is worth noting that the C1C2 used for NMR in this study contains five helices from ChR1 and only helix 6 and 7 of ChR2. The degree of light adaptation in the case of ChR1 and C1C2 is smaller than that for ChR2 but still substantial.[6] In contrast, some ChRs such as CaChR1 of *Chlamydomonas augustae* show very little light−dark adaptation.[43]

The IDA state is formed in darkness within several hours. Moreover, it appears that even low light intensities are required to convert the IDA to the DA_{app} state, which includes a mixture of two parent states with either all-*trans* or 13-*cis* retinal (Figure 9). In the absence of a photochemical *trans,anti*−13-*cis,syn*

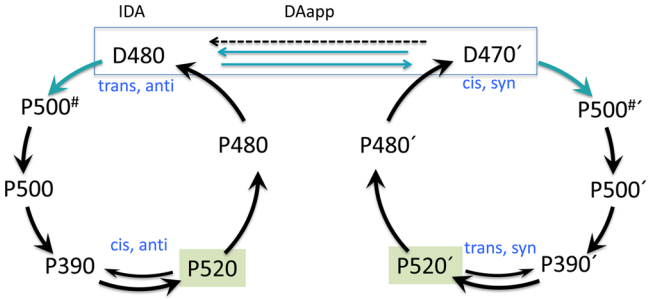

Figure 9. Photocycles of the all-*trans* and 13-*cis* forms of ChR2 and their interconversion. The blue and black arrows denote the photochemical and thermal reactions, respectively. The initial dark-adapted (IDA) state includes only the all-*trans* isomer (*trans,anti*), whereas the apparent dark-adapted (DA_{app}) state includes a mixture of all-*trans* and 13-*cis* isomers (*trans,anti* and *cis,syn*). The all-*trans* and 13-*cis* isomers undergo a photocycle initiated by all-*trans* to 13-*cis* and 13-cis to all-*trans* photoisomerization around the C(13)=C(14) bond, respectively. The 13-*cis* isomer of the DA_{app} state is slowly converted to the all-*trans* isomer via thermal isomerization. The two photocycles are most likely connected via photochemical (blue arrows) and thermal (dashed arrow) isomerization of the parent states (D480/D470′).

isomerization, thermal conversion should lead to a slow but steady decrease in the 13-*cis,syn* isomer population. Thus, the lack of such changes in the RR spectra measured at ambient temperatures suggests an efficient *trans,anti*−13-*cis,syn* isomerization while the sample resides in the laser beam.

On the basis of the RR experiments, the RSB isomers in DA_{app} were identified as all-*trans*, 15-*anti*, and 13-*cis*,15-*syn*, implying that the Schiff base proton adopts the same orientation in the chromophore pocket of both isomers, which is analogous to BR_{DA}.[46] Consequently, the all-*trans*,15-*anti* to 13-*cis*,15-*syn* photoisomerization is associated with minimal steric constraints by the protein environment, consistent with an efficient photoinduced conversion from IDA to DA_{app} that is accompanied by an only minimal shift in

DOI: 10.1021/acs.biochem.5b00597
Biochemistry 2015, 54, 5389−5400

UV−vis absorption. Thus, this *cis*−*trans* photoisomerization already occurs at very low light intensities, which constitutes a serious obstacle in determining the isomeric composition of IDA via spectroscopic experiments.

Photoinduced Processes of the all-*trans*,15-*anti* and 13-*cis*,15-*syn* Isomers of DA_{app}. The first intermediate of the DA_{app} photocycle is P500, which is formed within 2.7 ps at ambient temperature.[35] This species is different from P500 that converts into P390 on a microsecond time scale. Thus, we hypothesize the existence of an early P500 and a late P500 that may correlate with the K590 and L550 states of BR. Hence, we denote the "early" and "late" P500 of ChR2 as $P500^{\#}$ and P500, respectively. Whereas $P500^{\#}$ is easily converted back in the RR experiments at 80 K, the P500 intermediate is photochemically (more) stable and thus accumulates under photostationary conditions at 220 K. In contrast, the photoisomerization of $P500^{\#}$ is thus not associated with a thermal activation barrier.

Evidently, the relaxation of $P500^{\#}$ to P500 can be associated with only minor structural changes of the chromophore because, thus far, no spectral differences have been identified for the P500 states at "low" and "high" temperatures (4−80 and 80−220 K, respectively) or at early and late time scales despite differences in reactivity. A more detailed analysis requires the determination of the complete RR spectra of the two P500 states, which could not be obtained with the single-beam experiments employed in this work.

However, the RR spectra of the photostationary mixtures (DA_{app}/P500/P390) allow to detect formation of intermediates and concomitant depletion of the parent state that is associated with a change in the isomeric composition. At ambient temperature, formation of P500 and P390 is accompanied by a decrease in the level of the all-*trans* isomer in DA_{app} that is at least 4 times larger than that of the 13-*cis* isomer (Figure 6). At first sight, this finding might be taken as an indication that only the all-*trans* isomer is photoactive. This interpretation, however, should be discarded in light of the RR spectrum of the P390 intermediate. Unlike the M410 state of BR, in which the retinal adopts a uniform 13-*cis*,15-*anti* configuration, the chromophore composition in P390 (ChR) is heterogeneous as it includes a 13-*cis*,15-*anti* and an all-*trans*,15-*syn* deprotonated RSB. Although its spectrum was obtained from the slow-cycling mutant ChR2-C128S/D156A, extrapolation of these conclusions to the wild-type-like protein ChR2 is justified because the spectra of corresponding parent DA_{app} states are very similar (Figure S3). Thus, the unique kinetic properties of ChR2-C128S/D156A are not associated with different chromophore conformations.

The coexistence of two isomers in P390 implies that both the all-*trans*,15-*anti* and the 13-*cis*,15-*syn* isomers of the DA_{app} state are photoactive and that the photoisomerization step involves a rotation around the C(13)═C(14) bond in each case. Preferential depletion of the all-*trans* isomer of the DA_{app} state during the early photocycle events is more pronounced at ambient temperature than at 220 K (Figures 4 and 6). Thus, one may conclude that the quantum yield of photoisomerization of the 13-*cis*,15-*syn* isomer is smaller, and that the kinetics of the subsequent thermal relaxation step are slower than those of the all-*trans*,15-*anti* isomer. Moreover, the different photoreactivity of the two isomers in the DA_{app} state of ChR2 can be linked to specific interactions between the Schiff base and nearby water molecule(s). In fact, the crystal structure of the C1C2 IDA state shows a structural water molecule within 4.4 Å of the Schiff base.[14]

Altogether, these findings confirm previous conclusions that ChR undergoes two photocycles associated with the all-*trans* isomer and the 13-*cis* isomer of the DA_{app} state.[6,9,47,48] Thus, the individual intermediates probed by transient absorption spectroscopy always represent a mixture of the conjugate species involved in the all-*trans* and 13-*cis* photocycles (Figure 9). Both photocycles are most likely connected via the efficient photoconversion between the all-*trans* and 13-*cis* RSB isomers of the parent states. Thus, the previously proposed thermal transitions between the late conjugate intermediates of the two photocycles[9] are questioned, albeit not rigorously disproved. Further investigation is required to acquire a thorough understanding of this model.

The results obtained from the spectroscopic measurements performed in this study are relevant to the ChR photocurrents in the algae and host cells. We know that the early photocurrents during photostimulation of a previously dark adapted ChR (I_{peak}) are larger than steady-state currents in bright light, and that the early conducting state differs with respect to conductance and ion selectivity. This also holds true for the recently reported ChR2-like channelrhodopsin *Ps*ChR2 from *Platymonas subcordiformis*.[49,50] For ChR2, the early conductance is now interpreted as a photoproduct resulting from D480 only in case the protein has been fully dark-adapted (IDA), whereas the stationary current is mediated by two conducting states, one as a photoproduct of D480 with an all-*trans*,15-*anti* chromophore and the second as a photoproduct of the D470′ with the 13-*cis*,15-*syn* chromophore. For *P. subcordiformis*, the authors postulated two photocycles, whereas ChR molecules cycling through one of them were trapped in a late nonconducting intermediate.[49,50]

■ ASSOCIATED CONTENT

Supporting Information

The Supporting Information is available free of charge on the ACS Publications website at DOI: 10.1021/acs.biochem.5b00597.

Experimental details as well as absorption and resonance Raman spectroscopy data (PDF)

■ AUTHOR INFORMATION

Corresponding Authors

*E-mail: oschkinat@fmp-berlin.de.
*E-mail: hildebrandt@chem.tu-berlin.de.
*E-mail: katja.stehfest@cms.hu-berlin.de.

Author Contributions

S.B. and D.S. contributed equally to this work.

Funding

This work was supported by the German Research Foundation DFG (UniCat to P. Hildebrandt and P. Hegemann; SFB 1078 B1 to P. Hegemann and H.O., B6 to P. Hildebrandt).

Notes

The authors declare no competing financial interest.

■ ACKNOWLEDGMENTS

We acknowledge the technical support by E. Schlodder, R. Hagedorn, N. Erdmann, D. Michl, M. Beerbaum, and P. Schmieder.

DOI: 10.1021/acs.biochem.5b00597
Biochemistry 2015, 54, 5389−5400

REFERENCES

(1) Govorunova, E. G., Sineshchekov, O. A., and Hegemann, P. (1997) Desensitization and dark recovery of the photoreceptor current in Chlamydomonas reinhardtii. *Plant physiology 115*, 633−642.

(2) Ehlenbeck, S., Gradmann, D., Braun, F. J., and Hegemann, P. (2002) Evidence for a light-induced H+ conductance in the eye of the green alga Chlamydomonas reinhardtii. *Biophys. J. 82*, 740−751.

(3) Nagel, G., Szellas, T., Huhn, W., Kateriya, S., Adeishvili, N., Berthold, P., Ollig, D., Hegemann, P., and Bamberg, E. (2003) Channelrhodopsin-2, a directly light-gated cation-selective membrane channel. *Proc. Natl. Acad. Sci. U. S. A. 100*, 13940−13945.

(4) Schneider, F., Grimm, C., and Hegemann, P. (2015) Biophysics of Channelrhodopsin. *Annu. Rev. Biophys. 44*, 167−186.

(5) Sineshchekov, O. A., Litvin, F. F., and Keszthelyi, L. (1990) 2 Components of Photoreceptor Potential in Phototaxis of the Flagellated Green-Alga Haematococcus-Pluvialis. *Biophys. J. 57*, 33−39.

(6) Hegemann, P., Ehlenbeck, S., and Gradmann, D. (2005) Multiple Photocycles of Channelrhodopsin. *Biophys. J. 89*, 3911−3918.

(7) Schneider, F., Gradmann, D., and Hegemann, P. (2013) Ion Selectivity and Competition in Channelrhodopsins. *Biophys. J. 105*, 91−100.

(8) Stehfest, K., Ritter, E., Berndt, A., Bartl, F., and Hegemann, P. (2010) The Branched Photocycle of the Slow-Cycling Channelrhodopsin-2 Mutant C128T. *J. Mol. Biol. 398*, 690−702.

(9) Ritter, E., Piwowarski, P., Hegemann, P., and Bartl, F. J. (2013) Light-dark Adaptation of Channelrhodopsin C128T Mutant. *J. Biol. Chem. 288*, 10451−10458.

(10) Nack, M., Radu, I., Bamann, C., Bamberg, E., and Heberle, J. (2009) The retinal structure of channelrhodopsin-2 assessed by resonance Raman spectroscopy. *FEBS Lett. 583*, 3676−3680.

(11) Luck, M., Mathes, T., Bruun, S., Fudim, R., Hagedorn, R., Tran Nguyen, T. M., Kateriya, S., Kennis, J. T., Hildebrandt, P., and Hegemann, P. (2012) A photochromic histidine kinase rhodopsin (HKR1) that is bimodally switched by ultraviolet and blue light. *J. Biol. Chem. 287*, 40083−40090.

(12) Bruun, S., Naumann, H., Kuhlmann, U., Schulz, C., Stehfest, K., Hegemann, P., and Hildebrandt, P. (2011) The chromophore structure of the long-lived intermediate of the C128T channelrhodopsin-2 variant. *FEBS Lett. 585*, 3998−4001.

(13) Tsunoda, S. P., and Hegemann, P. (2009) Glu 87 of Channelrhodopsin-1 Causes pH-dependent Color Tuning and Fast Photocurrent Inactivation. *Photochem. Photobiol. 85*, 564−569.

(14) Kato, H. E., Zhang, F., Yizhar, O., Ramakrishnan, C., Nishizawa, T., Hirata, K., Ito, J., Aita, Y., Tsukazaki, T., Hayashi, S., Hegemann, P., Maturana, A. D., Ishitani, R., Deisseroth, K., and Nureki, O. (2012) Crystal structure of the channelrhodopsin light-gated cation channel. *Nature 482*, 369−U115.

(15) Elgeti, M., Kazmin, R., Heck, M., Morizumi, T., Ritter, E., Scheerer, P., Ernst, O. P., Siebert, F., Hofmann, K. P., and Bartl, F. J. (2011) Conserved Tyr223(5.58) plays different roles in the activation and G-protein interaction of rhodopsin. *J. Am. Chem. Soc. 133*, 7159−7165.

(16) Schlodder, E., Cetin, M., Byrdin, M., Terekhova, I. V., and Karapetyan, N. V. (2005) P700+- and 3P700-induced quenching of the fluorescence at 760 nm in trimeric Photosystem I complexes from the cyanobacterium Arthrospira platensis. *Biochim. Biophys. Acta, Bioenerg. 1706*, 53−67.

(17) Naumann, H., Klare, J. P., Engelhard, M., Hildebrandt, P., and Murgida, D. H. (2006) Time-resolved methods in Biophysics. 1. A novel pump and probe surface-enhanced resonance Raman approach for studying biological photoreceptors. *Photochem. Photobiol. Sci. 5*, 1103−1108.

(18) Lohrmann, R., and Stockburger, M. (1992) Time-Resolved Resonance Raman Studies of Bacteriorhodopsin and Its Intermediates K590 and L550: Biological Implications. *J. Raman Spectrosc. 23*, 575−583.

(19) Ly, H. K., Utesch, T., Díaz-Moreno, I., García-Heredia, J. M., De La Rosa, M. A., and Hildebrandt, P. (2012) Perturbation of the Redox Site Structure of Cytochrome c Variants upon Tyrosine Nitration. *J. Phys. Chem. B 116*, 5694−5702.

(20) Luck, M., Bruun, S., Hegemann, P., and Hildebrandt, P. (2015) Dark state of Histidin-Kinase-Rhodopsin-1. *FEBS Lett.*,.

(21) Bax, A. D., Griffey, R. H., and Hawkins, B. L. (1983) Correlation of proton and nitrogen-15 chemical shifts by multiple quantum NMR. *J. Magn. Reson. 55*, 301−315.

(22) Takegoshi, K., Nakamura, S., and Terao, T. (2001) Dipolar-assisted rotational resonance in magic-angle spinning NMR. *Chem. Phys. Lett. 344*, 631−637.

(23) Metz, G., Wu, X. L., and Smith, S. O. (1994) Ramped-Amplitude Cross Polarization in Magic-Angle-Spinning NMR. *J. Magn. Reson., Ser. A 110*, 219−227.

(24) Pines, A. (1972) Proton-Enhanced Nuclear Induction Spectroscopy. A Method for High Resolution NMR of Dilute Spins in Solids. *J. Chem. Phys. 56*, 1776.

(25) Fung, B. M., Khitrin, A. K., and Ermolaev, K. (2000) An improved broadband decoupling sequence for liquid crystals and solids. *J. Magn. Reson. 142*, 97−101.

(26) Song, C., Hu, K.-N., Joo, C.-G., Swager, T. M., and Griffin, R. G. (2006) TOTAPOL: A Biradical Polarizing Agent for Dynamic Nuclear Polarization Experiments in Aqueous Media. *J. Am. Chem. Soc. 128*, 11385−11390.

(27) Patzelt, H., Ulrich, A. S., Egbringhoff, H., Düx, P., Ashurst, J., Simon, B., Oschkinat, H., and Oesterhelt, D. (1997) Towards structural investigations on isotope labelled native bacteriorhodopsin in detergent micelles by solution-state NMR spectroscopy. *J. Biomol. NMR 10*, 95−106.

(28) Linden, A. H., Franks, W. T., Akbey, U., Lange, S., Rossum, B.-J., and Oschkinat, H. (2011) Cryogenic temperature effects and resolution upon slow cooling of protein preparations in solid state NMR. *J. Biomol. NMR 51*, 283−292.

(29) Kalisky, O., Goldschmidt, C. R., and Ottolenghi, M. (1977) On the photocycle and light adaptation of dark-adapted bacteriorhodopsin. *Biophys. J. 19*, 185−189.

(30) Alshuth, T., and Stockburger, M. (1981) Structural Changes in the Retinal Chromophore of Bacteriorhodopsin Studied by Resonance Raman Spectroscopy. *Ber. Bunsenges. Phys. Chem. 85*, 484−489.

(31) Heyde, M. E., Gill, D., Kilponen, R. G., and Rimai, L. (1971) Raman spectra of Schiff bases of retinal (models of visual photoreceptors). *J. Am. Chem. Soc. 93*, 6776−6780.

(32) Diller, R., and Stockburger, M. (1988) Kinetic Resonance Raman Studies Reveal Different Conformational States of Bacteriorhodopsin. *Biochemistry 27*, 7641−7651.

(33) Ames, J. B., Fodor, S. P., Gebhard, R., Raap, J., van den Berg, E. M., Lugtenburg, J., and Mathies, R. A. (1989) Bacteriorhodopsin's M412 intermediate contains a 13-cis, 14-s-trans, 15-anti-retinal Schiff base chromophore. *Biochemistry 28*, 3681−3687.

(34) Ernst, O. P., Lodowski, D. T., Elstner, M., Hegemann, P., Brown, L. S., and Kandori, H. (2014) Microbial and animal rhodopsins: structures, functions, and molecular mechanisms. *Chem. Rev. 114*, 126−163.

(35) Verhoefen, M. K., Bamann, C., Blocher, R., Forster, U., Bamberg, E., and Wachtveitl, J. (2010) The Photocycle of Channelrhodopsin-2: Ultrafast Reaction Dynamics and Subsequent Reaction Steps. *ChemPhysChem 11*, 3113−3122.

(36) Smith, S. O., Braiman, M. S., Myers, A. B., Pardoen, J. A., Courtin, J. M. L., Winkel, C., Lugtenburg, J., and Mathies, R. A. (1987) Vibrational Analysis of the All-Trans-Retinal Chromophore in Light-Adapted Bacteriorhodopsin. *J. Am. Chem. Soc. 109*, 3108−3125.

(37) Gilson, H. S., Honig, B. H., Croteau, A., Zarrilli, G., and Nakanishi, K. (1988) Analysis of the Factors That Influence the C = N Stretching Frequency of Polyene Schiff Bases. Implications for Bacteriorhodopsin and Rhodopsin. *Biophys. J. 53*, 261−269.

(38) Smith, S. O., Pardoen, J. A., Lugtenburg, J., and Mathies, R. A. (1987) Vibrational Analysis of the 13-Cis-Retinal Chromophore in Dark-Adapted Bacteriorhodopsin. *J. Phys. Chem. 91*, 804−819.

DOI: 10.1021/acs.biochem.5b00597
Biochemistry 2015, 54, 5389−5400

(39) Hildebrandt, P., and Stockburger, M. (1984) Role of Water in Bacteriorhodopsin's Chromophore: Resonance Raman Study. *Biochemistry 23*, 5539−5548.
(40) Woutersen, S., and Bakker, H. J. (1999) Resonant Intermolecular Transfer of Vibrational Energy in Liquid Water. *Nature 402*, 507−509.
(41) Yizhar, O., Fenno, L. E., Prigge, M., Schneider, F., Davidson, T. J., O'Shea, D. J., Sohal, V. S., Goshen, I., Finkelstein, J., Paz, J. T., Stehfest, K., Fudim, R., Ramakrishnan, C., Huguenard, J. R., Hegemann, P., and Deisseroth, K. (2011) Neocortical excitation/inhibition balance in information processing and social dysfunction. *Nature 477*, 171−178.
(42) Smith, S. O., Myers, A. B., Mathies, R. A., Pardoen, J. A., Winkel, C., van den Berg, E. M., and Lugtenburg, J. (1985) Vibrational analysis of the all-trans retinal protonated Schiff base. *Biophys. J. 47*, 653−664.
(43) Ogren, J. I., Manaev, S., Russano, D., Li, H., and Spudich, J. L. (2014) Retinal Chromophore Structure and Schiff Base Interaction in Red-Shifted Channelrhodopsin from *Chlamydomonas augustae*. *Biochemistry 53*, 3961−3970.
(44) Beckmann, M., and Hegemann, P. (1991) Invitro Identification of Rhodopsin in the Green-Alga Chlamydomonas. *Biochemistry 30*, 3692−3697.
(45) Lawson, M. a., Zacks, D. N., Derguini, F., Nakanishi, K., and Spudich, J. L. (1991) Retinal Analog Restoration of Photophobic Responses in a Blind Chlamydomonas-Reinhardtii Mutant - Evidence for an Archaebacterial Like Chromophore in a Eukaryotic Rhodopsin. *Biophys. J. 60*, 1490−1498.
(46) Patzelt, H., Simon, B., terLaak, A., Kessler, B., Kuhne, R., Schmieder, P., Oesterhelt, D., and Oschkinat, H. (2002) The structures of the active center in dark-adapted bacteriorhodopsin by solution-state NMR spectroscopy. *Proc. Natl. Acad. Sci. U. S. A. 99*, 9765−9770.
(47) Grossman, N., Nikolic, K., Toumazou, C., and Degenaar, P. (2011) Modeling Study of the Light Stimulation of a Neuron Cell With Channelrhodopsin-2 Mutants. *IEEE Trans. Biomed. Eng. 58*, 1742−1751.
(48) Nikolic, K., Grossman, N., Grubb, M. S., Burrone, J., Toumazou, C., and Degenaar, P. (2009) Photocycles of Channelrhodopsin-2. *Photochem. Photobiol. 85*, 400−411.
(49) Szundi, I., Li, H., Chen, E., Bogomolni, R., Spudich, J. L., and Kliger, D. S. (2015) Platymonas subcordiformis Channelrhodopsin-2 Function: I. THE PHOTOCHEMICAL REACTION CYCLE. *J. Biol. Chem. 290*, 16573−16584.
(50) Szundi, I., Bogomolni, R., and Kliger, D. S. (2015) Platymonas subcordiformis Channelrhodopsin-2 (PsChR2) Function: II. RELATIONSHIP OF THE PHOTOCHEMICAL REACTION CYCLE TO CHANNEL CURRENTS. *J. Biol. Chem. 290*, 16585−16594.

DOI: 10.1021/acs.biochem.5b00597
Biochemistry 2015, 54, 5389−5400